Article

Safety Analysis of a Nuclear Power Plant against Unexpected Tsunamis

Byung-Ho Kim [ID] **, Min-Jong Song and Yong-Sik Cho *** [ID]

Department of Civil and Environmental Engineering, Hanyang University, Seoul 04763, Korea
* Correspondence: ysc59@hanyang.ac.kr

Abstract: The East Sea (Sea of Japan), surrounded by Korea, Japan, and Russia, is highly vulnerable to catastrophic tsunamis. Several nuclear power plants (NPPs) operate along the eastern coast of Korea and several more are under construction. Unexpected tsunamis can affect these power plants. The safety of NPPs has attracted worldwide attention since the Fukushima NPP accident. In this study, a coupled numerical model comprising propagation and run-up models was employed to investigate the safety of an NPP against unexpected tsunami attacks. The maximum and minimum tsunami heights and arrival times of the leading tsunami were numerically predicted to ensure the safety of the Uljin NPP, where six plants are already operational and two more are under construction. The predicted numerical results were compared with the safety guidelines proposed by relevant authorities. These results indicate that NPPs are reasonably safe from unexpected tsunamis. Additionally, we confirmed that the tsunami heights and arrival times of a leading tsunami becomes smaller and delayed as the latitude of the epicenter increased.

Keywords: nuclear power plant; numerical simulation; logic tree approach; safety analysis; tsunami

1. Introduction

The tsunamis generated by impulsive undersea earthquakes are one of the most devastating threats to coastal communities. To establish countermeasures for tsunamis and risk assessments, most tsunami research has focused on tsunami-prone areas where people live or work, such as coastal regions and nuclear power plant (NPP) sites. For example, many researchers have developed tsunami early warning systems [1,2], created tsunami hazard maps [3,4], and conducted probabilistic tsunami hazard assessments (PTHA) by using a logic tree approach to evaluate the probability of exceeding tsunami heights [5,6]. Researchers have also conducted wave ray tracing to examine the bathymetric effects on tsunami propagation paths [7–9].

The 2004 Indian Ocean tsunami, 2010 Chilean tsunami, and 2011 Great East Japan tsunami caused losses of human lives, property damage, and building destruction [10,11]. Specifically, the number of human deaths in the 2011 tsunami event with a magnitude (M_w) of 9.0 was 15,868, with over 2800 people missing. The direct financial damage exceeded 300 billion dollars and 120,000 buildings were destroyed. Furthermore, the tsunami inundation caused a cooling system failure at the Fukushima NPP, resulting in a nuclear meltdown and several hydrogen explosions. Therefore, the maximum and minimum tsunami heights are critical in NPP operations.

Currently, 24 NPPs are operational in South Korea. Among these, 18 NPPs are located on the eastern coast of Korea and are vulnerable to tsunamis. In this study, we considered the Uljin NPP, located close to the Imwon Port, as the study area. The most destructive tsunami in South Korea in the past 100 years was the 1983 tsunami event (1983 East Sea tsunami), with the highest damage recorded at Imwon Port. Ref. [12] performed a safety analysis of the Uljin NPP against the 1983 tsunami event for the maximum and minimum

tsunami heights and arrival times of the leading tsunami (hereinafter, the arrival times of the leading tsunami are simply referred to as "arrival times").

Tsunamis have occurred during last 100 years in various epicenters of the East Sea (Sea of Japan) and can occur in various epicenters in the future. Therefore, to adequately address the corresponding uncertainty of tsunami hazards, tsunami heights and arrival times must be analyzed for various tsunami events containing historical and virtual unexpected tsunamis. In this study, we investigated the maximum tsunami heights, minimum tsunami heights, and arrival times using a larger number of tsunami events (historical and unexpected tsunamis) than [12], and it is necessary to analyze the distribution of tsunami heights according to the location of the epicenter for tsunami mitigation plans. Thus, this study was organized as follows: (1) investigating the tsunami events containing fault parameters used for the initial conditions of tsunami modeling; (2) conducting wave ray tracing for selected cases of tsunami events; (3) applying the logic tree approach to consider the uncertainty; (4) numerically simulating the tsunami(s); (5) conducting a safety analysis of the Uljin NPP; (6) analysis of tsunami heights and arrival times according to the latitude of the epicenter.

2. Tsunami Events

Tsunami occurrences are relatively rare compared to other natural disasters, such as typhoon or floods. Therefore, observation data of previous tsunamis are generally used for validation. On the other hand, virtual tsunamis that can occur in the future are used for tsunami risk assessment.

For numerical simulation, a tsunami comprising nine fault parameter variables needed to be investigated in this study. The fault parameters were used to generate the initial water surface displacement of the tsunami during the numerical simulation. The initial water surface displacement of the tsunami, an essential initial condition of the numerical simulation, was reproduced using Mansinha and Smylie's method [13]. We investigated the historical and virtual tsunamis containing the fault parameters used in the numerical simulation.

Tsunamis have occurred in the East Sea (Sea of Japan) for centuries. Among these, four tsunami events occurred in the 1900s [14]. Table A1 shows the fault parameters of the four historical tsunami events along the East Sea, where longitude and latitude represent the location of the epicenter (tsunamis' occurrence site), H denotes the height at the top of the fault plane, θ is the strike angle, δ is the dip angle, λ is the slip angle, L is the length, W is the width, and D is the dislocation where the plane is displaced (Figure 1). Additionally, 71 virtual tsunami events (unexpected tsunamis) as suggested by the Korean Peninsula Energy Development Organization [15] and the Ministry of Land, Infrastructure, Transport, and Tourism [14] were investigated (Tables A2 and A3). Totally, we considered 75 tsunami events for NPP safety analysis.
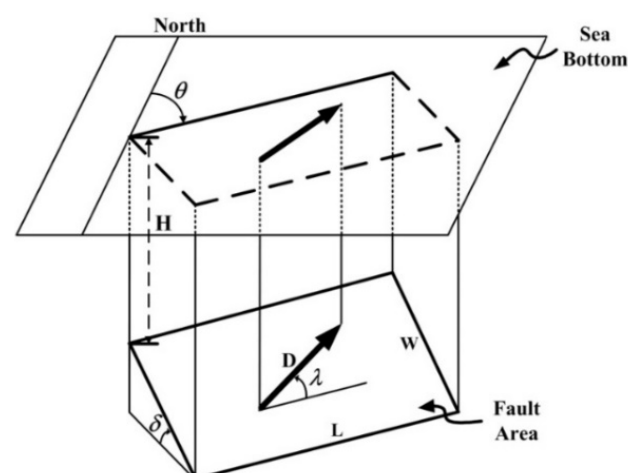

Figure 1. Definition of fault parameters.

3. Selecting Tsunami Events for Numerical Simulation

3.1. Wave Ray Tracing

The tsunamis propagating long distances along the East Sea from the epicenter located in the west coast of Japan are highly affected by the bottom topography [7]. Ref. [7] and [9] applied wave ray tracing to tsunamis to examine the impacts of bathymetry during tsunami propagation. They showed that the propagation paths of tsunami waves could be estimated.

In this study, the wave ray tracing suggested by [7] was adopted, and simulations of wave ray tracing were performed for 75 historical and virtual tsunami events in order to confirm whether the tsunami propagation paths at the Uljin NPP are focusing or defocusing. Wave ray focusing means that high tsunami heights can be measured at the Uljin NPP. Therefore, the cases for the numerical simulations of tsunamis were determined by considering the results from the wave ray tracing. The topographic and bathymetric data used in the numerical modeling were purchased from the "National Geographic Information Institute" and "Korea Hydrographic and Oceanographic Agency," respectively. The wave rays were generated at $1°$ to identify the focusing and defocusing in the Uljin NPP area.

3.2. Logic Tree Approach

The logic tree approach, which is contained in PTHA, can evaluate uncertainty in tsunami hazards [5,6,16,17]. Thus, many researchers conduct the logic tree approach in tsunami research. Uncertainty can be classified as either aleatory or epistemic. Aleatory uncertainty is defined as uncertainty caused by the randomness of nature, such as the fault slip distribution of an earthquake event, the location of the epicenter, or the condition of the tide at the time of a tsunami event [18]. Ref. [17] analyzed the importance of aleatory uncertainty in tsunami hazards by using a logic tree approach for an Oregon seaside. They considered three M_w values using a logic tree approach: 8.8, 9.0, and 9.2. In addition, three slip shape parameters and eight peak slips were considered for each moment magnitude. By following this process containing the logic tree approach, numerical simulations were performed for a total of 72 tsunami events to estimate five intensity measures (maximum inundation, maximum velocity, maximum momentum flux, arrival time, and duration exceeding a 1 m inundation depth). Epistemic uncertainty is defined as uncertainty caused by incomplete knowledge and data about the earthquake process, such as initial deformation of the ground motion from the earthquake: slip angle (λ), dip angle (δ), and strike angle (θ). The Japan Society of Civil Engineers [19] suggested a range of fault parameter values for applying the logic tree approach on the East Sea (Sea of Japan). However, the logic tree approach is not governed by a single method and can be applied in various ways depending on the researcher. For example, when considering the M_w values of tsunami events, there is no standard regulation regarding the interval, e.g., whether it needs to be set at 0.1, 0.2, or any other value.

In this study, we used 75 tsunami events for considering aleatory uncertainty and adopted the logic tree approach in order to consider epistemic uncertainty. Additionally, the tsunami event with a probable maximum earthquake M_w (8.0) along the East Sea was considered based on the literature [14,15,19]. To apply the logic tree, a tsunami event containing the fault parameters of an earthquake was produced as a new tsunami event and applied with set values for the M_w, dip angle (δ), and strike angle (θ).

4. Numerical Model

In this study, a coupled numerical model was used for tsunami simulation at the Uljin NPP. The coupled model comprises a long-distance tsunami propagation model and an inundation process (run-up and run-down) model for the area along the shorelines, named HYCEL-NAMI and HYCEL-RUNUP, respectively. The HYCEL models were improved based on the Cornell multigrid coupled tsunami model (COMCOT). The HYCEL models consist of HYCEL-NAMI, which can consider the dispersion effect during tsunami wave propagation in deep water, and HYCEL-RUNUP, which can consider the shoaling effect containing bottom friction in shallow water. Detailed descriptions of the COMCOT model

and the HYCEL model are provided in the literature [20,21]. For the numerical simulation, we used numerical domains divided into six sub-domains (A-F), as shown in Figure 2. The mesh details of each domain are given in Table 1.
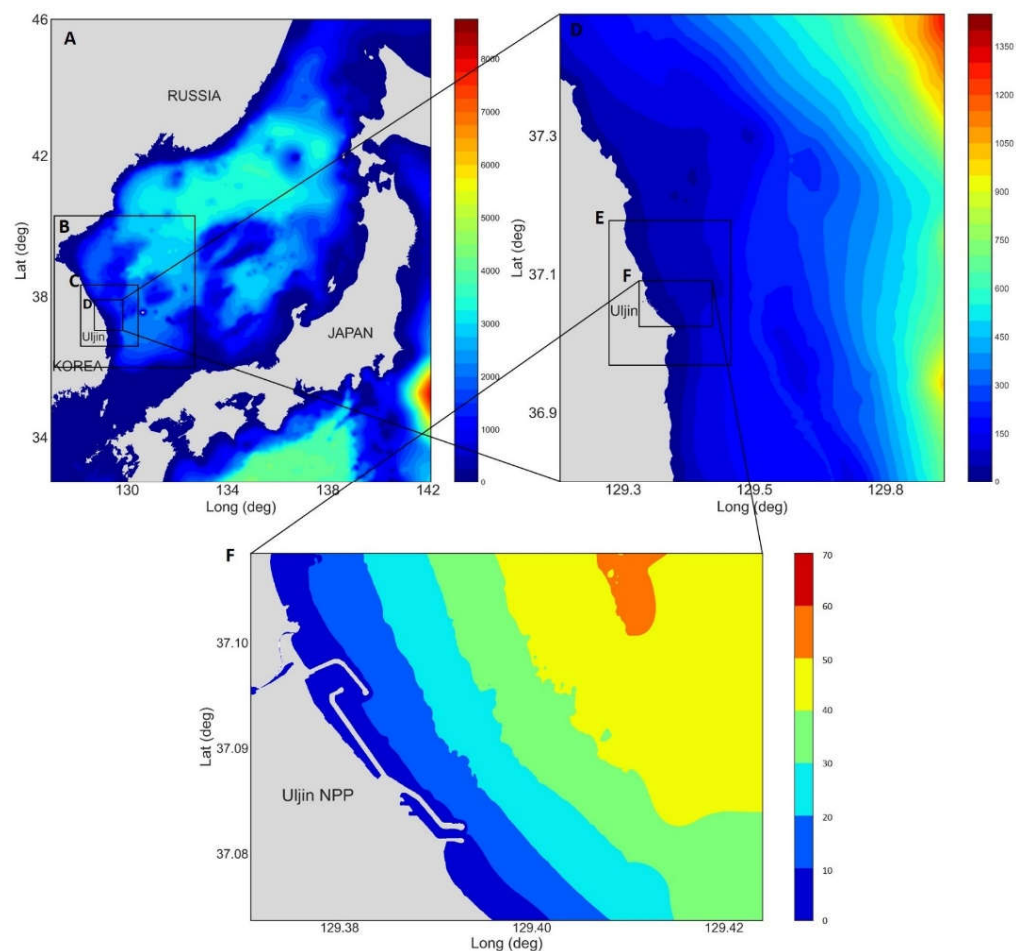
Figure 2. Computational domains (A–F) and bathymetry of East Sea.

Table 1. Computational mesh details of domains.

Region	Grid Size (m)	Mesh Number		Time Step Size (s)	Type of Numerical Model
		x	y		
A	1215	1092	1383	3.00	
B	405	1204	1306	1.00	Propagation
C	135	1204	1306	0.33	
D	45	1303	1504	0.11	
E	15	1105	1285	0.04	Inundation
F	5	1066	697	0.04	

4.1. Propagation Model (HYCEL-NAMI)

A tsunami is a wave that can travel long distances and strike neighboring and distant coastal communities. As tsunami propagation progresses, the dispersion effect becomes important, whereas the nonlinear convective terms can be ignored because the free-surface displacement with propagation is less than the water depth. For this reason, linear Boussinesq equations are generally recommended for modeling tsunami propagation [22]. However, linear Boussinesq equations containing dispersion terms present a complication in terms of numerical discretization. To resolve this numerical difficulty, [21] proposed a

propagation model using a scheme that discretized linear shallow water equations using a leapfrog scheme based on the finite difference method. We used a propagation model in four sub-domains (A–D). The linear shallow water equations used in the propagation modeling are as follows:

$$\frac{\partial \zeta}{\partial t} + \frac{\partial P}{\partial x} + \frac{\partial Q}{\partial y} = 0$$

$$\frac{\partial P}{\partial t} + gh\frac{\partial \zeta}{\partial x} = 0$$

$$\frac{\partial Q}{\partial t} + gh\frac{\partial \zeta}{\partial y} = 0$$

where ζ denotes the free-surface displacement, h is the mean water depth, g is the force of gravity, and P and Q are the volume fluxes in the x and y directions, respectively.

4.2. Inundation Model (HYCEL-RUNUP)

Linear shallow water equations are not adequate for the nearshore, where the wavelengths of incident tsunamis become smaller than their amplitudes. As the amplitude of tsunamis increases, the nonlinear convective inertia force and bottom friction terms become important. In contrast, the dispersion terms and Coriolis force no longer play vital roles. Consequently, nonlinear shallow water equations, including bottom friction effects, are adequate for tsunami modeling in the nearshore and run-up processes of tsunamis [22]. We used an inundation model in two sub-domains (E-F). The nonlinear shallow water equations are as follows:

$$\frac{\partial \zeta}{\partial t} + \frac{\partial P}{\partial x} + \frac{\partial Q}{\partial y} = 0$$

$$\frac{\partial P}{\partial t} + \frac{\partial}{\partial x}\left(\frac{P^2}{H}\right) + \frac{\partial}{\partial y}\left(\frac{PQ}{H}\right) + gh\frac{\partial \zeta}{\partial x} + \tau x H = 0$$

$$\frac{\partial Q}{\partial t} + \frac{\partial}{\partial x}\left(\frac{PQ}{H}\right) + \frac{\partial}{\partial y}\left(\frac{Q^2}{H}\right) + gh\frac{\partial \zeta}{\partial x} + \tau y H = 0$$

where H is the total depth and τ_x and τ_y are the bottom frictional terms in the x and y directions, respectively. Detailed descriptions of the equations and numerical techniques are provided in the literature [21,22].

5. Results

5.1. Wave Ray Tracing and Logic Tree Approach

Wave ray tracing was performed to investigate 75 cases (historical and virtual tsunami events) using MATLAB code from [23]. Figure 3 shows the wave ray results for several cases in this study. In the case of the 1983 tsunami, K05, and F20, quite a number of wave propagation paths reached the Uljin NPP (Figure 3a), whereas in other cases, the paths relatively rarely reached the Uljin NPP (Figure 3b). Thus, we considered 12 cases (Figure 4) with M_w values higher than 7.7; this was based on a M_w of 7.7, which corresponded to the highest damage in South Korea (Imwon port) in 1983. The locations of the twelve considered cases and detailed information on each fault parameter are shown in Figure 4 and Table 2.
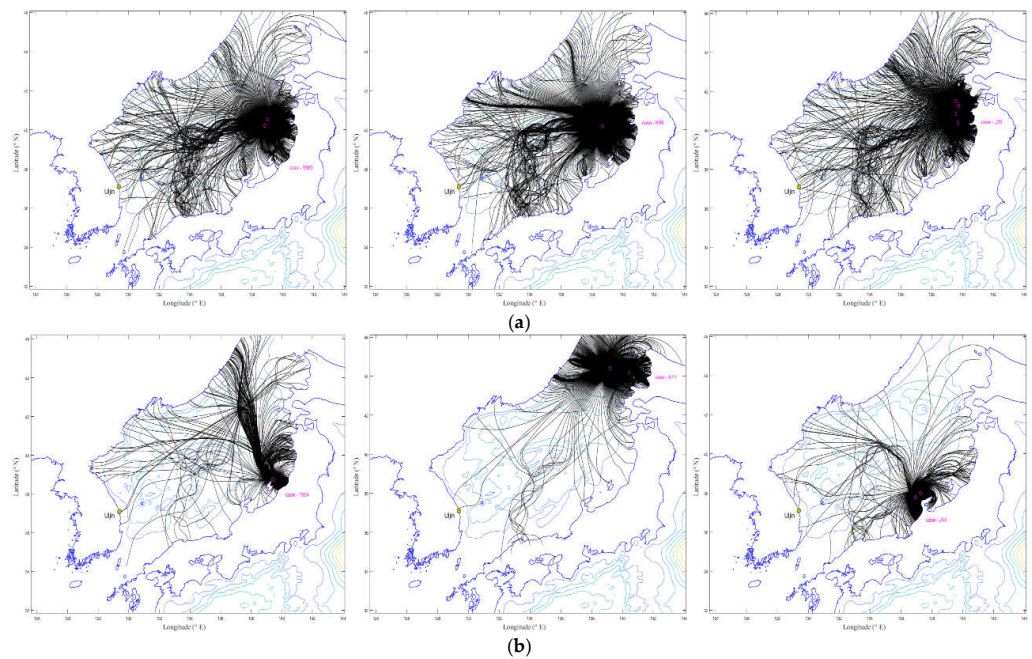
Figure 3. Wave ray tracing results. (**a**) Considered cases: 1983 historical tsunami, K05 virtual tsunami, and F20 virtual tsunami. (**b**) Unconsidered cases: 1964 historical tsunami, K11 virtual tsunami, and F44 virtual tsunami.

Table 2. Fault parameters of twelve tsunami events.

| Classification | Source Location | | H (km) | θ (°) | δ (°) | λ (°) | L (km) | W (km) | D (m) | M_w |
	Longitude (°E)	Latitude (°N)								
Case 1 (F34)	139.7	39.1	1.1	211.0	45.0	106.0	71.9	19.7	5.5	7.7
	139.3	38.5	1.1	197.0	45.0	97.0	52.0	19.7	5.5	
Case 2 (F28)	138.9	40.0	2.3	200.0	45.0	115.0	35.7	18.0	5.18	7.7
	138.7	39.7	2.3	185.0	45.0	93.0	39.7	18.0	5.18	
	138.7	39.4	2.3	202.0	45.0	118.0	50.9	18.0	5.18	
Case 3 (1983)	138.8	40.2	2.0	22.0	40.0	90.0	40.0	30.0	7.6	7.7
	139.0	40.5	3.0	355.0	25.0	80.0	60.0	30.0	3.1	
Case 4 (F18)	139.8	40.9	2.2	7.0	45.0	95.0	100.0	18.1	5.5	7.7
	139.9	41.8	2.2	348.0	45.0	87.0	37.4	18.1	5.5	
Case 5 (F20)	139.6	41.5	2.0	151.0	45.0	68.0	30.8	18.4	6.0	7.8
	139.7	41.3	2.0	199.0	45.0	102.0	47.2	18.4	6.0	
	139.6	40.8	2.0	165.0	45.0	103.0	52.4	18.4	6.0	
	139.7	40.4	2.0	175.0	45.0	88.0	39.2	18.4	6.0	
Case 6 (F19)	138.2	40.9	4.3	33.0	30.0	110.0	58.6	27.3	6.0	7.8
	138.6	41.3	4.3	18.0	30.0	97.0	42.8	27.3	6.0	
Case 7 (F17)	139.4	41.0	2.8	10.0	45.0	106.0	53.9	21.5	6.0	7.8
	139.5	41.5	2.8	350.0	45.0	96.0	81.0	21.5	6.0	
Case 8 (F14)	139.6	43.4	3.6	195.0	45.0	99.0	43.3	20.3	6.0	7.8
	139.4	43.1	3.6	192.0	45.0	111.0	79.6	20.3	6.0	
	139.2	42.4	3.6	167.0	60.0	105.0	51.9	16.6	6.0	

Table 2. *Cont.*

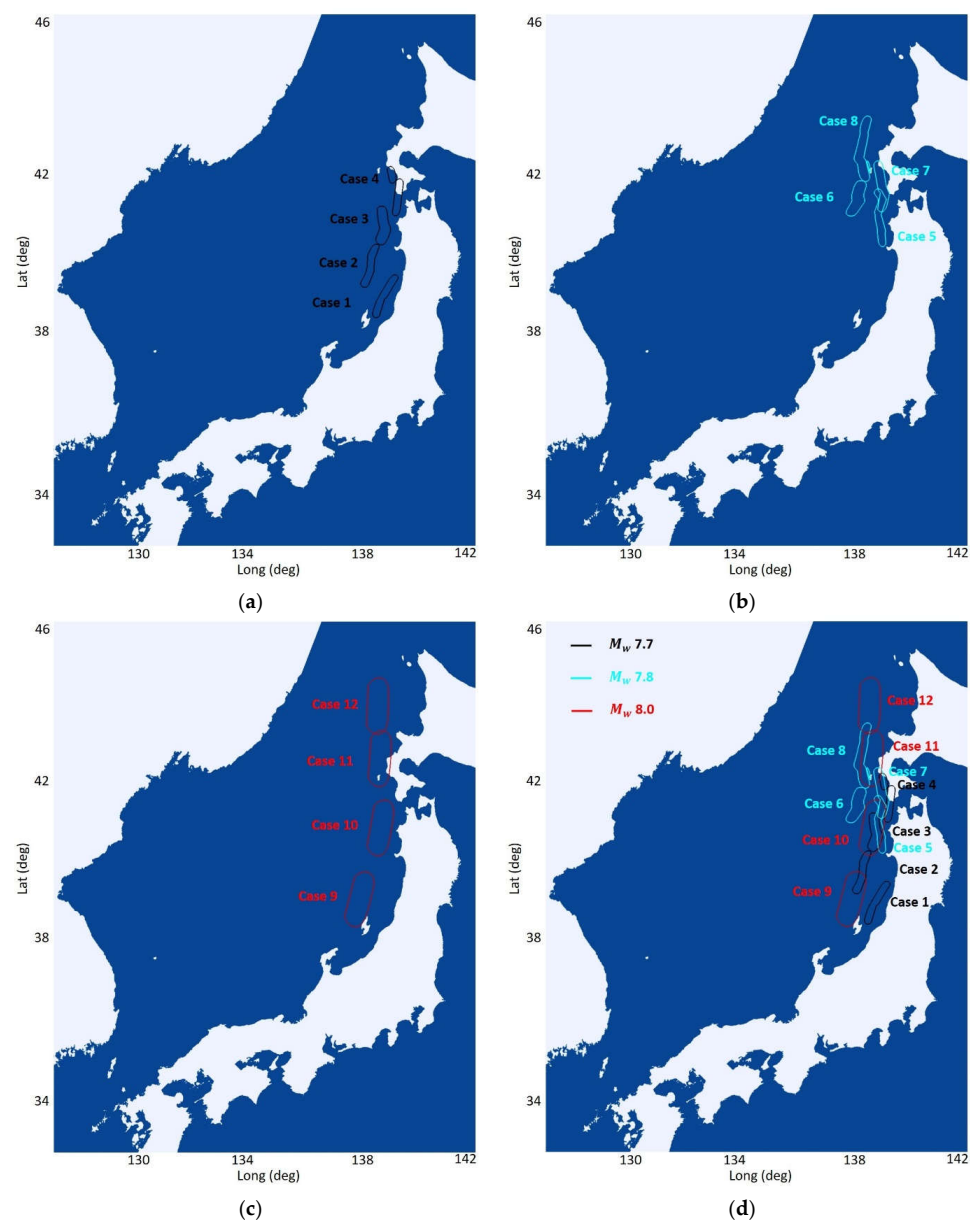| Classification	Source Location		H (km)	θ (°)	δ (°)	λ (°)	L (km)	W (km)	D (m)	M_w
	Longitude (°E)	Latitude (°N)								
Case 9 (K02)	137.5	37.5	1.0	14.5	40.0	90.0	125.8	62.9	6.3	8.0
Case 10 (K05)	138.7	40.2	1.0	10.0	40.0	90.0	125.8	62.9	6.3	8.0
Case 11 (K08)	139.1	42.1	1.0	4.0	40.0	90.0	125.8	62.9	6.3	8.0
Case 12 (K10)	139.2	43.5	1.0	2.0	40.0	90.0	125.8	62.9	6.3	8.0

Figure 4. Location of twelve considered tsunami events. (**a**) M_w = 7.7. (**b**) M_w = 7.8. (**c**) M_w = 8.0. (**d**) All tsunami events.

The logic tree approach was applied to generate tsunami events to consider the epistemic uncertainty of the tsunami hazards. The 12 cases were separated into three branches: M_w, dip angle (δ), and strike angle (θ). The M_w, dip angle, and strike angle scales were set at ±0.1 (the KEDO cases, which indicated an M_w 8.0, were set down to an M_w 7.8 using interval −0.1), ±15°, and ±10° intervals, respectively. Ref. [19] suggested ranges of over +30° to +60° and from −30° to +30° for the dip and strike angles in the East Sea, respectively. Some of the 12 cases considered in this study had a dip angle lower than 30° or higher than 60° but we applied a range of dip angles within ±15° to evaluate the epistemic uncertainty of the tsunami hazard in more detail. Consequently, 27 branches (tsunami events) were generated from one case; in total, we generated 324 new cases by using the logic tree approach to perform the numerical simulations (Figure 5).
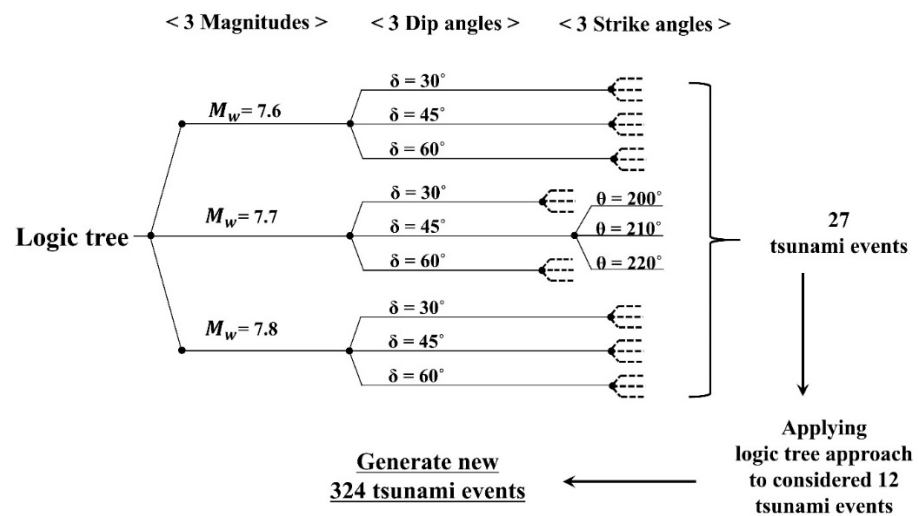
Figure 5. Outline of the logic tree approach in this research.

5.2. Safety Analysis of a Nuclear Power Plant

The results comprised the maximum tsunami heights, minimum tsunami heights, and arrival times at the Uljin NPP for the safety analysis of the tsunami hazards. The data were predicted at a gauge in front of the intake structure (Figure 6) to determine whether a cooling water supply was possible in the intake structure.

Figure 6. Location of gauge in Uljin Nuclear Power Plant.

The maximum and minimum tsunami heights of the 324 cases increased as M_w increased (Figure 7). The M_w value of 8.0 showed a wider interquartile range (IQR) than other M_w values at the maximum tsunami heights. However, the IQRs were similar for the minimum tsunami heights. The median of the maximum tsunami heights increased as M_w increased, although the results for the M_w of 7.6 in the minimum tsunami heights were higher than those for 7.7 (Figure 7b). The highest maximum tsunami height predicted among the 324 cases was approximately + 3.9 m (Figure 7a). This indicates that the Uljin NPP site is safe from tsunami inundation because the site elevation is 10.0 m above the mean sea level (Figure 8). As shown in Figure 7b, the minimum tsunami height was predicted to be approximately −3.6 m. The intake structure was shut down when the minimum tsunami height was lower than the lowest allowable elevation of the essential service water pump (−4.6 m). Thus, the intake structure at the Uljin NPP can be considered safe against historical and virtual tsunami events.

(**a**)

(**b**)
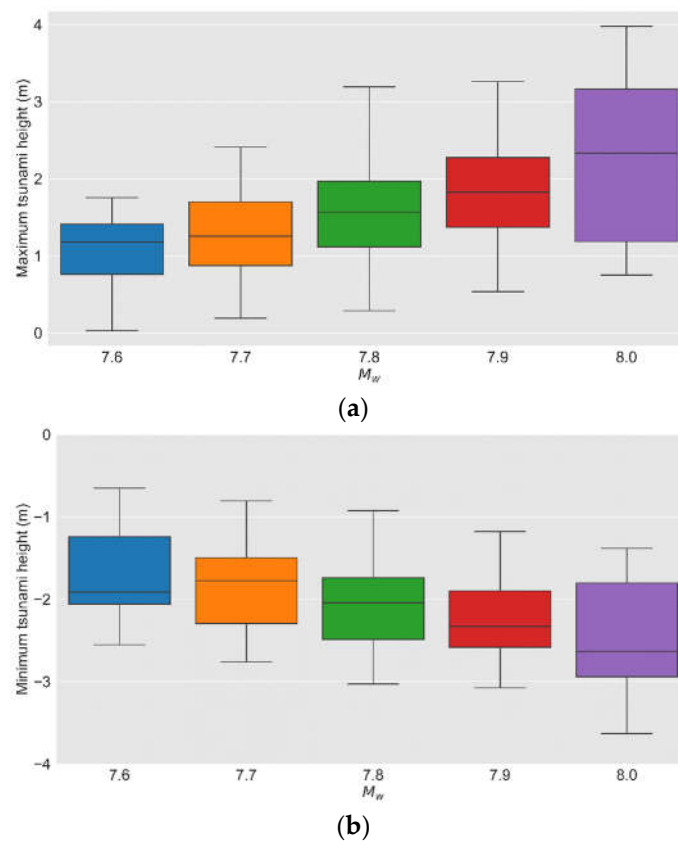
Figure 7. Box plots of tsunami heights by magnitude (M_w). (**a**) Maximum tsunami heights. (**b**) Minimum tsunami heights.

Figure 9 shows the maximum and minimum tsunami heights for the 12 tsunami cases (M_w 7.7, 7.8, and 8.0), each containing 27 branches. Case 1–Case 8 (original M_w 7.7 and 7.8) were constructed by making a new branch, using an interval of $M_w \pm 0.1$ from the original case with the logic tree approach, and Case 9–Case 12 (original M_w 8.0) were constructed using an interval of $M_w − 0.1$ (down to M_w 7.8). The results show that the maximum and minimum tsunami heights decreased as the latitude of the epicenter increased, except for Cases 3 and 7 (Figure 9).
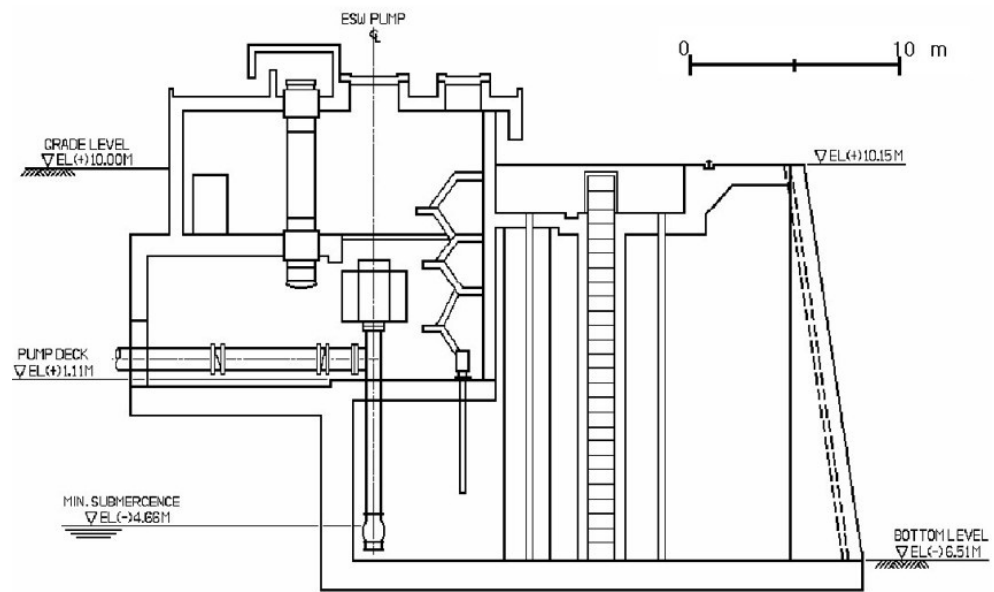
Figure 8. Main elevations of the Uljin Nuclear Power Plant.

(**a**)

(**b**)
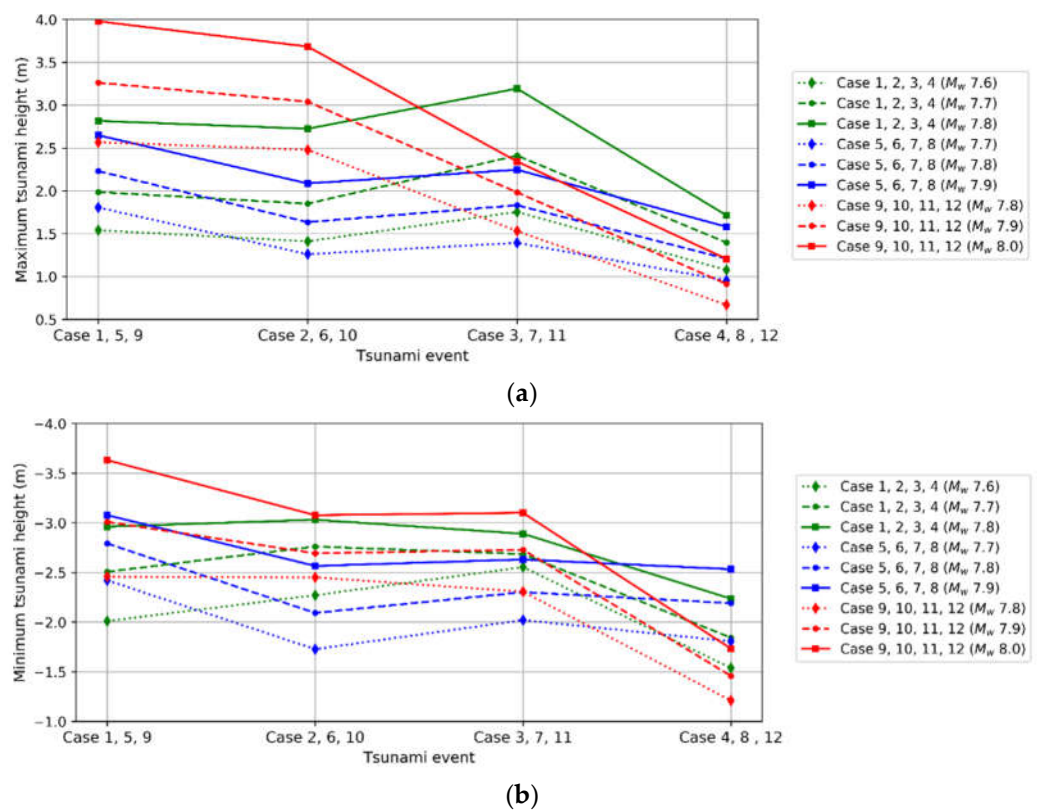
Figure 9. Maximum and minimum tsunami heights for twelve considered tsunami events. (**a**) Maximum tsunami heights. (**b**) Minimum tsunami heights.

The arrival time representing the leading tsunami is useful for considering counter-measures or evacuation plans and is generally considered by tsunami researchers. In this study, arrival times were between 103 and 138 min for all 324 cases (Table 3). In general, 30 min is defined as an appropriate amount of time for evacuating people in response to a tsunami triggered by undersea earthquakes in the East Sea [24]. Thus, the arrival times for the 324 cases (historical and virtual tsunamis) are sufficient for the evacuation of people at the Uljin NPP.

Table 3. Arrival time results of twelve cases.

Classification	Arrival Time Range (Min)	Remark
Case 1	127–138	
Case 2	111–120	
Case 3	119–123	
Case 4	128–131	
Case 5	121–126	
Case 6	112–114	Each case contains 27 branches
Case 7	125–130	
Case 8	121–123	
Case 9	103–107	
Case 10	116–119	
Case 11	119–123	
Case 12	131–132	

5.3. Analysis of Tsunami Heights and Arrival Times According to Latitude of Epicenter

To confirm the trend of decreasing tsunami heights according to the latitude of the epicenter, cases with the same M_w value of 7.8 were considered the highest M_w values for historical tsunami events in the East Sea [14]. We considered the latitude of the epicenter, which can more easily figure out the characteristics of tsunami events instead of the distance to the epicenter to investigate results (tsunami heights and arrival times). These properties can highly affect wave propagation by bottom topography of the East Sea. Among the 12 cases shown in Figure 4, certain cases (M_w of 7.8) were located at a similar location (latitude), and we considered cases with higher tsunami heights. Consequently, six cases were selected (Figure 10). The results of the six cases with the same M_w value (7.8) show that the maximum and minimum tsunami heights decreased as the latitude of the epicenter increased, except for the maximum tsunami height of Case 3, shown in Figure 10. The results for the six cases exhibit two trends. First, Cases 1, 2, and 3, with relatively high maximum tsunami heights, were predicted to reach over +2.5 m, whereas Cases 7, 11, and 12 were predicted to be less than +2.0 m high (Figure 11). The spatial distributions of the calculated maximum tsunami heights for the six cases are shown in Figure 12. For Cases 1, 2, and 3 (Figure 12a–c), a high tsunami height for the Uljin NPP was predicted, whereas for Cases 7, 11, and 12 (Figure 12d–f), a relatively low tsunami height was predicted. Additionally, we performed probability density function (PDF) analysis and cumulative distribution function (CDF) analysis using Weibull distribution on the tsunami heights. The Weibull distribution was identified as the best fit for predicted tsunami heights along the East Sea [25]. Figure 13 shows the PDF and CDF made from maximum and minimum tsunami heights. By comparing the plots, it can be noted that the maximum and minimum tsunami height becomes smaller as the latitude of the epicenter increases, especially in Group 1 (Case 1, Case 2, and Case 3) and Group 2 (Case 7, Case 11, and Case 12). Therefore, in the future, increased attention needs to be given to potential tsunamis that may occur at the latitudes corresponding to Cases 1–3 rather than to potential tsunamis occurring elsewhere.
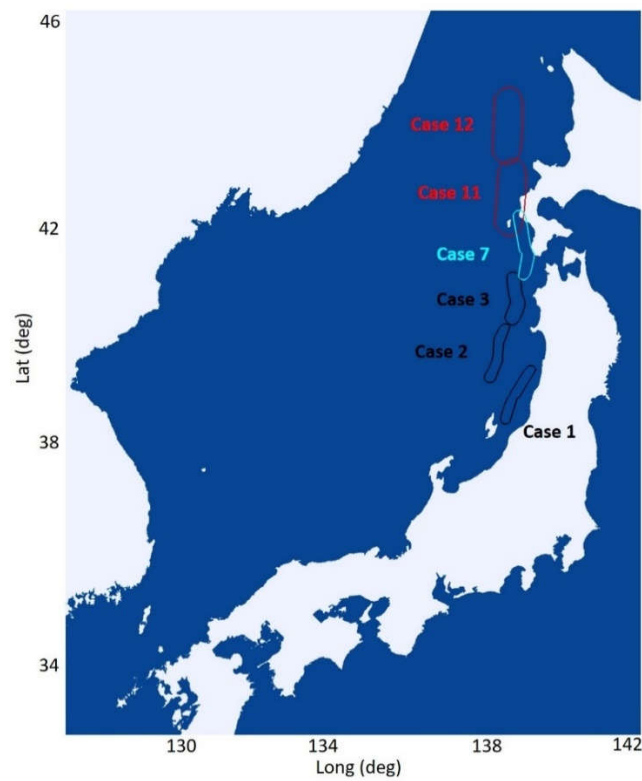
Figure 10. Locations of six tsunami events (M_w 7.8).
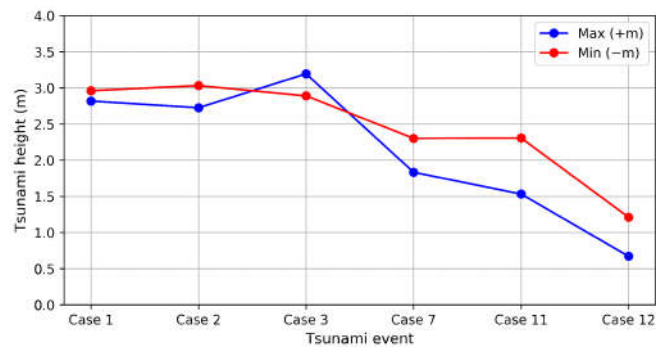
Figure 11. Maximum and minimum tsunami height for six tsunami events.
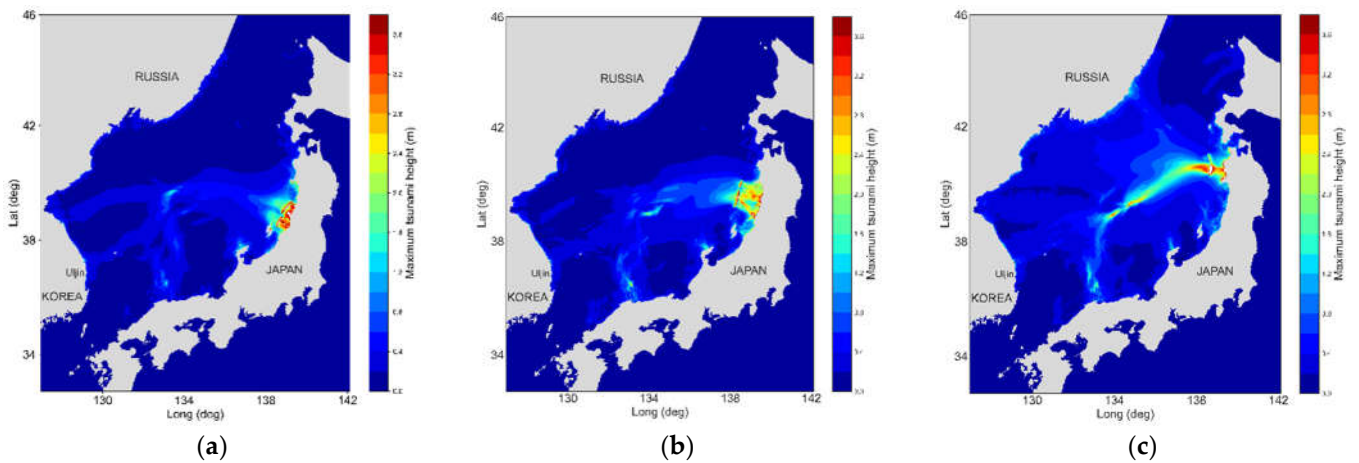
Figure 12. *Cont*.
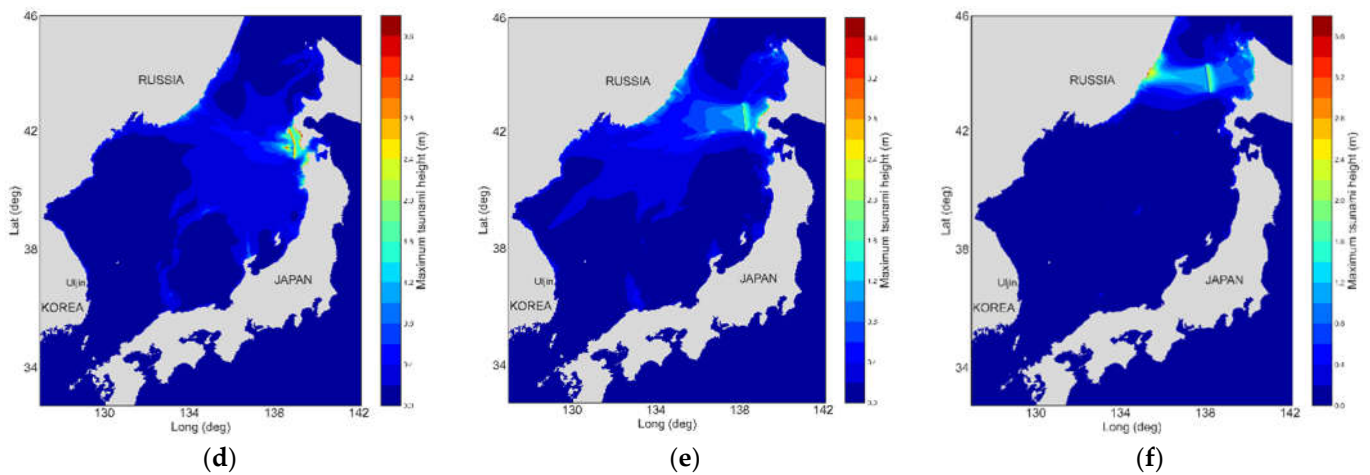
Figure 12. Spatial distribution of calculated maximum tsunami height (blue color represents still water level (SWL)). (**a**) Case 1. (**b**) Case 2. (**c**) Case 3. (**d**) Case 7. (**e**) Case 11. (**f**) Case 12.
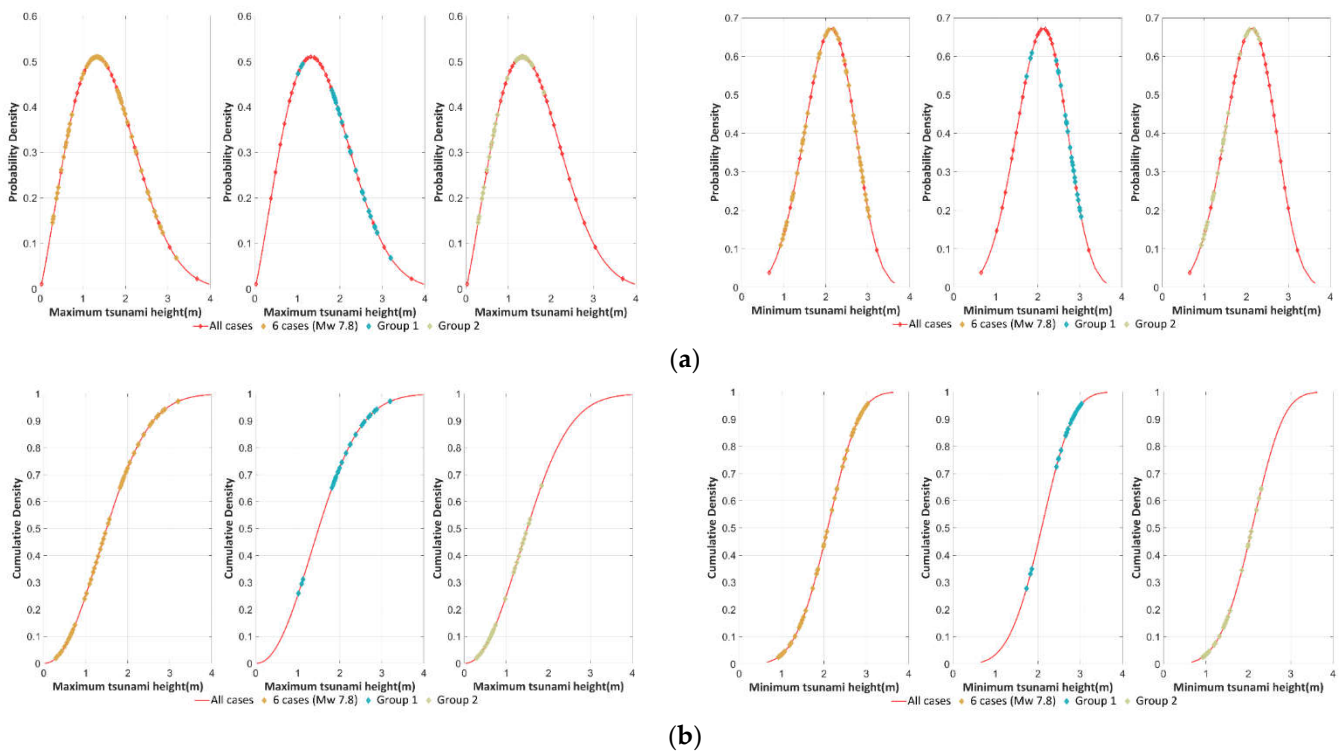
Figure 13. PDF and CDF of maximum and minimum tsunami heights. (**a**) PDF for maximum tsunami heights and minimum tsunami heights (All cases: 324 cases. 6 cases: Case 1, Case 2, Case 3, Case 7, Case 11, and Case 12; Group 1: Case 1, Case 2, and Case 3; Group 2: Case 7, Case 11, and Case 12). (**b**) CDF for maximum tsunami heights and minimum tsunami heights (All cases: 324 cases. 6 cases (M_w 7.8): Case 1, Case 2, Case 3, Case 7, Case 11, and Case 12; Group 1 (M_w 7.8): Case 1, Case 2, and Case 3; Group 2 (M_w 7.8): Case 7, Case 11, and Case 12).

We analyzed the trend of the arrival times according to the latitude of the epicenter. The arrival times were typically delayed as the latitude of the epicenter increased among the six cases, with the exception of a few outcomes, such as Case 1 and Case 11 (Table 4). Case 1, located closer to the Uljin NPP than the other cases, was predicted to be the slowest. Figure 14a,b show the tsunami wave propagation for Cases 1 and 11 after 30, 70, and 100 min, respectively. As shown in Figure 14, the leading wave of Case 11 is faster than that of Case 1, even though the epicenter of Case 11 is farther from the Uljin NPP than

that of Case 1. This result indicates that the leading wave of the tsunami in Case 1 was affected by the bottom topography, such as the Yamato Rise located in the middle of the East Sea, whereas Case 11 was affected relatively less than Case 1. Ref. [26] also confirmed the differences in arrival times owing to the influence of the Yamato Rise. Thus, the arrival times can be affected by the bottom topography of the East Sea, such as the Yamato Rise, depending on the case.

Table 4. Arrival time results for six cases with the same Mw 7.8.

	Classification		Arrival Time Range (Min)
Case 1	Longitude (°E)	139.7	127–138
		139.3	
	Latitude (°N)	39.1	
		38.5	
Case 2	Longitude (°E)	138.9	111–120
		138.7	
		138.7	
	Latitude (°N)	40.0	
		39.7	
		39.4	
Case 3	Longitude (°E)	138.8	119–123
		139.0	
	Latitude (°N)	40.2	
		40.5	
Case 7	Longitude (°E)	139.4	125–130
		139.5	
	Latitude (°N)	41.0	
		41.5	
Case 11	Longitude (°E)	139.1	119–123
	Latitude (°N)	42.1	
Case 12	Longitude (°E)	139.2	131–132
	Latitude (°N)	43.5	

(a)

Figure 14. *Cont.*

(**b**)
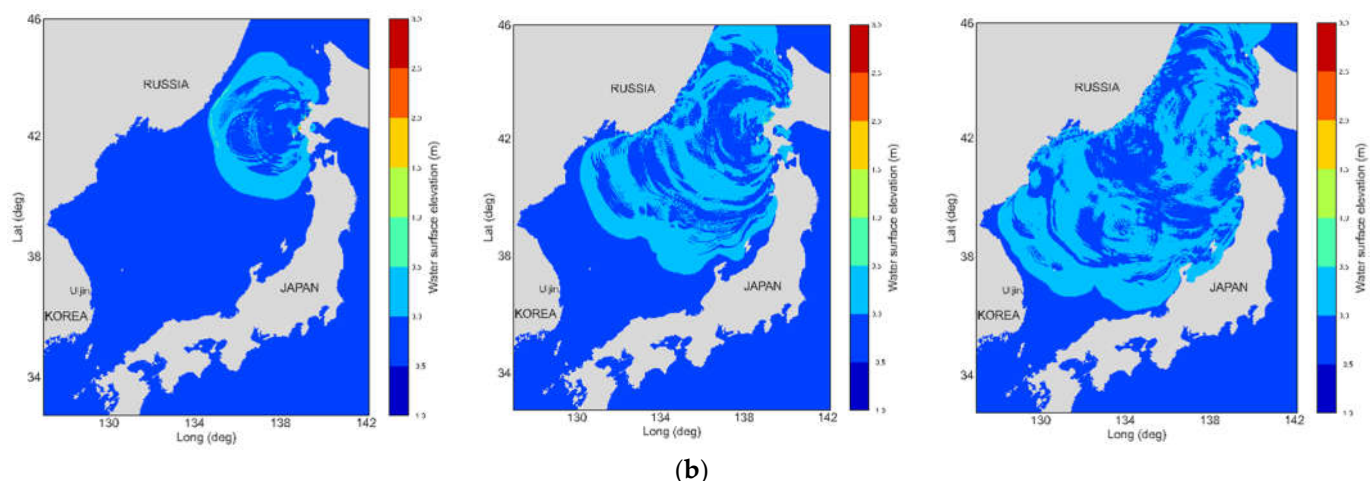
Figure 14. Tsunami wave propagation after 30, 70, and 100 min. (**a**) Case 1. (**b**) Case 11.
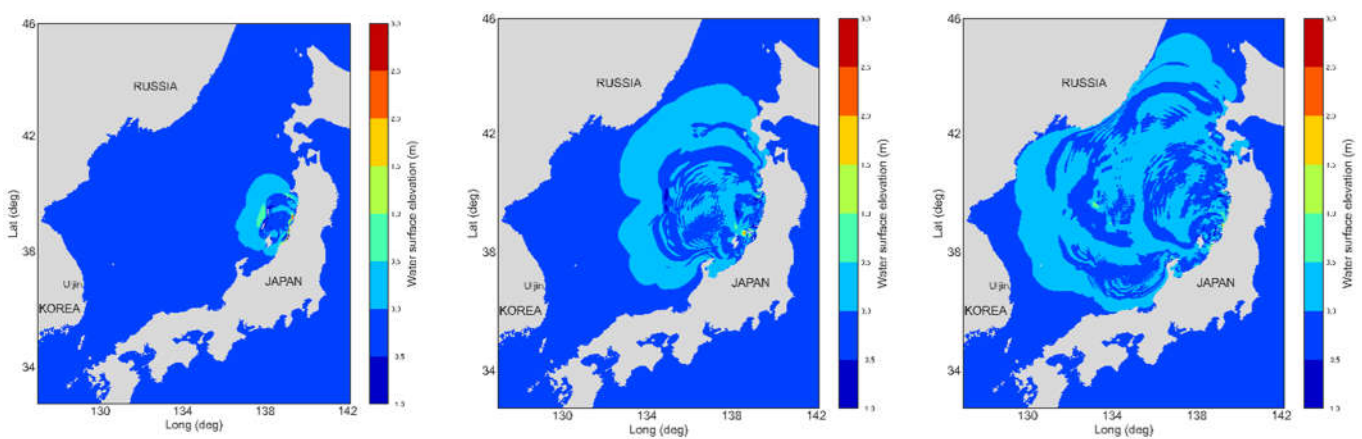
6. Conclusions

In this study, the maximum and minimum tsunami height results satisfied the safety guidelines for inundation and the lowest allowable elevation at the Uljin NPP for 324 cases (both historical and virtual tsunamis). The arrival times for the East Sea indicate that they provide sufficient time to evacuate people in response to tsunami events.

In general, as the latitude of the epicenter increased, the maximum and minimum tsunami heights decreased, and the arrival times were delayed. However, certain cases have shown different results. Considering the maximum tsunami heights, Case 3 was higher than all of the other cases occurring in other locations. In addition, Case 3 (M_w 7.8) was predicted to be higher than Cases 5, 6, 7, 8, 11, and 12 (M_w 7.9 and 8.0). Thus, the tsunamis potentially occurring in and around the epicenter in Case 3 may have had greater impacts on the Uljin NPP than potential tsunamis in other regions; therefore, greater attention must be paid to them. Second, considering the arrival times, tsunamis that occurred nearby did not always arrive first at the Uljin NPP. This means that arrival times can be affected by the bottom topography of the East Sea, such as the Yamato Rise, depending on the case. We only focused on the Uljin NPP in this study; on the other hand, future work could focus on further investigating other regions. Examples of studies that focused on other regions are provided in the literature [6,27].

To incorporate epistemic uncertainty, we employed a logic tree approach that considered three values: the M_w, dip angle (δ), and strike angle (θ). In a future study, we will conduct a sensitivity analysis of the M_w, dip angle, strike angle, and other fault parameters. Through a sensitivity analysis, the relevance of each fault parameter value can be validated and additional cases (tsunami events) considering the epistemic uncertainty can be generated according to the importance of each parameter. Finally, a PTHA can be performed at the Uljin NPP using the numerical simulation results generated with the additional branches.

Author Contributions: Investigation, B.-H.K.; Methodology, M.-J.S. and Y.-S.C.; Visualization, B.-H.K.; Writing—original draft, B.-H.K.; Writing— review & editing, M.-J.S. and Y.-S.C. All authors have read and agreed to the published version of the manuscript.

Institutional Review Board Statement: Not applicable.

Informed Consent Statement: Not applicable.

Data Availability Statement: Not applicable.

Appendix A

Table A1. Fault parameters of historical tsunami events.

| Classification | | Source Location | | H (km) | θ (°) | δ (°) | λ (°) | L (km) | W (km) | D (m) | M_w |
		Longitude (°E)	Latitude (°N)								
Historical tsunamis	1940	139.5	43.7	1.0	347.0	40.0	90.0	100.0	35.0	1.5	7.4
	1964	139.4	38.7	1.0	189.0	56.0	90.0	80.0	30.0	3.3	7.5
	1983	138.8	40.21	2.0	22.0	40.0	90.0	40.0	30.0	7.6	7.7
		139.0	40.54	3.0	355.0	25.0	80.0	60.0	30.0	3.1	
	1993	139.3	42.10	5.0	163.0	60.0	105.0	24.5	25.0	12.1	7.8
		139.2	42.34	5.0	175.0	60.0	105.0	30.0	25.0	2.5	
		139.4	43.13	10.0	188.0	35.0	80.0	90.0	25.0	5.7	

Table A2. Fault parameters of virtual tsunami events (Korean Energy Development Organization (KEDO), 1999).

| Classification | | Source Location | | H (km) | θ (°) | δ (°) | λ (°) | L (km) | W (km) | D (m) | M_w |
		Longitude (°E)	Latitude (°N)								
Virtual Tsunami (KEDO)	K01	137.5	37.5	1.0	0.0	40.0	90.0	125.8	62.9	6.3	8.0
	K02	137.7	38.3		14.5						
	K03	138.0	39.0		27.5						
	K04	138.4	39.7		17.0						
	K05	138.7	40.2		10.0						
	K06	138.9	40.9		1.0						
	K07	139.0	41.7		1.0						
	K08	139.1	42.1		4.0						
	K09	139.1	42.9		2.0						
	K10	139.2	43.5		2.0						
	K11	139.2	44.4		3.0						

Table A3. Fault parameters of virtual tsunami events (Ministry of Land, Infrastructure, Transport, and Tourism (MLIT), 2014).

| Classification | | Source Location | | H (km) | θ (°) | δ (°) | λ (°) | L (km) | W (km) | D (m) | M_w |
		Longitude (°E)	Latitude (°N)								
Virtual Tsunami (MLIT)	F01	141.8	44.8	1.1	340.0	45.0	78.0	46.5	7.0	6.0	7.9
		141.6	45.2	1.1	351.0	45.0	84.0	47.9	7.0	6.0	
		141.5	45.6	1.1	342.0	45.0	79.0	67.6	7.0	6.0	
		141.8	44.8	6.0	340.0	30.0	84.0	46.5	18.0	6.0	
		141.6	45.2	6.0	351.0	30.0	88.0	47.9	18.0	6.0	
		141.5	45.6	6.0	342.0	30.0	84.0	67.6	18.0	6.0	

Table A3. *Cont.*

Classification	Source Location		H (km)	θ (°)	δ (°)	λ (°)	L (km)	W (km)	D (m)	M_w
	Longitude (°E)	Latitude (°N)								
F02	141.0	45.2	1.4	355.0	45.0	82.0	53.7	19.3	5.2	
	140.9	45.7	1.4	23.0	45.0	100.0	36.3	19.3	5.2	7.7
	141.1	46.0	1.4	7.0	45.0	89.0	27.6	19.3	5.2	
F03	140.6	44.7	1.2	19.0	45.0	105.0	44.6	19.5	2.9	7.2
F04	139.7	44.7	1.7	34.0	45.0	138.0	58.4	18.8	3.3	7.3
F05	139.4	44.5	2.2	7.0	45.0	79.0	53.5	18.7	3.1	7.3
F06	140.7	44.3	1.5	217.0	45.0	82.0	42.0	19.1	4.7	
	140.4	44.0	1.5	191.0	45.0	79.0	62.5	19.1	4.7	7.6
F07	139.6	44.6	2.4	176.0	45.0	54.0	29.0	17.9	3.7	
	139.6	44.3	2.4	201.0	45.0	76.0	21.6	17.9	3.7	7.4
	139.5	44.1	2.4	167.0	45.0	48.0	25.3	17.9	3.7	
F08	140.2	44.1	2.0	218.0	45.0	93.0	31.3	18.4	3.8	
	140.0	43.9	2.0	189.0	45.0	77.0	20.9	18.4	3.8	7.4
	139.9	43.7	2.0	153.0	45.0	63.0	23.1	18.4	3.8	
F09	139.2	43.7	4.0	347.0	30.0	103.0	24.4	27.9	4.8	
	139.1	43.9	4.0	2.0	30.0	104.0	29.2	27.9	4.8	7.6
	139.1	44.2	4.0	347.0	30.0	103.0	18.8	27.9	4.8	
F10	139.7	43.7	3.4	194.0	45.0	98.0	73.2	20.6	3.9	7.5
F11	139.3	44.0	4.2	180.0	45.0	67.0	78.1	19.5	4.0	7.5
F12	139.9	43.4	1.8	156.0	45.0	62.0	24.0	18.7	3.7	
	140.0	43.2	1.8	161.0	45.0	65.0	29.3	18.7	3.7	7.4
	140.1	43.0	1.8	177.0	45.0	79.0	19.7	18.7	3.7	
F13	139.5	42.7	3.0	172.0	45.0	70.0	53.4	21.2	3.3	7.3
F14	139.6	43.4	3.6	195.0	45.0	99.0	43.3	20.3	6.0	
	139.4	43.1	3.6	192.0	45.0	111.0	79.6	20.3	6.0	7.8
	139.2	42.4	3.6	167.0	60.0	105.0	51.9	16.6	6.0	
F15	139.4	43.5	3.8	173.0	45.0	97.0	45.2	20.1	6.0	
	139.4	43.1	3.8	192.0	45.0	111.0	79.6	20.1	6.0	7.8
	139.2	42.4	3.8	167.0	60.0	105.0	51.9	16.4	6.0	
F16	138.7	41.7	4.6	14.0	30.0	94.0	75.9	26.7	4.8	7.6
F17	139.4	41.0	2.8	10.0	45.0	106.0	53.9	21.5	6.0	
	139.5	41.5	2.8	350.0	45.0	96.0	81.0	21.5	6.0	7.8
F18	139.8	40.9	2.2	7.0	45.0	95.0	100.0	18.1	5.5	
	139.9	41.8	2.2	348.0	45.0	87.0	37.4	18.1	5.5	7.7
F19	138.2	40.9	4.3	33.0	30.0	110.0	58.6	27.3	6.0	
	138.6	41.3	4.3	18.0	30.0	97.0	42.8	27.3	6.0	7.8

Table A3. *Cont.*

Classification		Source Location		H (km)	θ (°)	δ (°)	λ (°)	L (km)	W (km)	D (m)	M_w
		Longitude (°E)	Latitude (°N)								
	F20	139.6	41.5	2.0	151.0	45.0	68.0	30.8	18.4	6.0	7.8
		139.7	41.3	2.0	199.0	45.0	102.0	47.2	18.4	6.0	
		139.6	40.8	2.0	165.0	45.0	103.0	52.4	18.4	6.0	
		139.7	40.4	2.0	175.0	45.0	88.0	39.2	18.4	6.0	
	F21	139.6	41.5	2.4	151.0	45.0	68.0	30.8	17.9	3.8	7.4
		139.7	41.3	2.4	199.0	45.0	102.0	47.2	17.9	3.8	
	F22	13.96	40.9	2.6	1.0	45.0	98.0	63.9	17.5	3.3	7.3
	F23	139.6	40.8	1.7	165.0	45.0	103.0	52.4	18.8	4.3	7.5
		139.7	40.4	1.7	175.0	45.0	88.0	39.2	18.8	4.3	
Virtual Tsunami (MLIT)	F24	138.9	40.1	3.9	21.0	30.0	74.0	53.7	28.2	6.0	7.9
		139.2	40.6	3.9	349.0	30.0	80.0	77.9	28.2	6.0	
	F25	138.8	40.3	3.7	205.0	45.0	116.0	49.5	20.2	3.1	7.3
	F26	139.6	40.0	1.3	184.0	45.0	85.0	70.9	19.4	3.7	7.4
	F27	139.0	39.6	1.6	184.0	45.0	82.0	56.3	18.9	3.2	7.3
	F28	138.9	40.0	2.3	200.0	45.0	115.0	35.7	18.0	5.18	7.7
		138.7	39.7	2.3	185.0	45.0	93.0	39.7	18.0	5.18	
		138.7	39.4	2.3	202.0	45.0	118.0	50.9	18.0	5.18	
	F29	138.3	39.5	3.5	25.0	45.0	100.0	61.6	16.3	3.1	7.3
	F30	139.9	39.8	1.3	202.0	45.0	98.0	96.1	19.3	6.0	7.8
		139.4	39.0	1.3	247.0	45.0	120.0	56.5	19.3	6.0	
	F31	139.9	39.8	1.2	202.0	45.0	98.0	96.1	19.5	4.5	7.6
	F32	139.4	39.0	1.5	247.0	45.0	120.0	56.5	19.0	3.2	7.3
	F33	139.4	39.3	1.7	234.0	45.0	123.0	89.1	18.8	4.2	7.5
	F34	139.7	39.1	1.1	211.0	45.0	106.0	71.9	19.7	5.5	7.7
		139.3	38.5	1.1	197.0	45.0	97.0	52.0	19.7	5.5	
	F35	138.9	40.0	1.4	200.0	45.0	96.0	99.1	19.2	5.0	7.6
	F36	138.3	38.3	1.5	4.0	45.0	46.0	31.3	19.1	3.2	7.3
		138.3	38.6	1.5	36.0	45.0	97.0	23.6	19.1	3.2	
	F37	138.5	38.9	1.7	227.0	45.0	130.0	33.9	18.8	3.8	7.4
		138.1	38.7	1.7	185.0	45.0	90.0	41.0	18.8	3.8	
	F38	138.8	38.2	1.3	209.0	45.0	95.0	62.6	23.6	3.9	7.5
	F39	138.1	37.7	2.3	350.0	45.0	67.0	37.3	18.0	3.7	7.4
		138.0	38.1	2.3	38.0	45.0	73.0	36.9	18.0	3.7	
	F40	138.3	37.4	1.6	26.0	45.0	84.0	14.7	18.9	2.8	7.2
		138.4	37.6	1.6	338.0	45.0	66.0	27.7	18.9	2.8	
	F41	137.6	37.0	1.9	37.0	45.0	76.0	51.5	22.7	4.7	7.6
		137.9	37.4	1.9	55.0	45.0	102.0	34.1	22.7	4.7	

Table A3. *Cont.*

Classification		Source Location		H (km)	θ (°)	δ (°)	λ (°)	L (km)	W (km)	D (m)	M_w
		Longitude (°E)	Latitude (°N)								
	F42	137.9	38.0	2.5	201.0	45.0	78.0	37.7	17.7	3.1	7.3
		137.7	37.7	2.5	241.0	45.0	112.0	18.1	17.7	3.1	
	F43	136.7	37.3	1.1	64.0	45.0	113.0	48.3	19.7	4.5	7.6
		137.2	37.5	1.1	55.0	45.0	105.0	45.9	19.7	4.5	
	F44	137.3	38.0	1.2	230.0	45.0	99.0	36.0	19.6	3.1	7.3
		137.0	37.8	1.2	267.0	45.0	145.0	13.7	19.6	3.1	
	F45	137.3	37.2	2.0	228.0	45.0	103.0	16.2	18.3	2.7	7.2
		137.2	37.1	2.0	191.0	45.0	62.0	26.4	18.3	2.7	
	F46	136.6	37.1	1.1	177.0	60.0	42.0	26.0	13.0	2.1	6.9
	F47	136.1	36.7	1.4	30.0	60.0	107.0	42.5	15.8	2.6	7.1
	F48	135.7	37.0	2.1	81.0	60.0	215.0	28.2	14.1	2.1	6.9
	F49	134.8	36.5	2.4	81.0	60.0	264.0	21.1	14.5	3.6	7.4
		135.0	36.6	2.4	47.0	60.0	145.0	36.3	14.5	3.6	
		135.3	36.8	2.4	54.0	60.0	215.0	29.9	14.5	3.6	
	F50	136.0	36.5	1.2	39.0	60.0	126.0	23.7	11.8	2.0	6.8
	F51	136.1	36.4	1.2	232.0	60.0	145.0	48.0	16.0	2.7	7.2
	F52	136.1	35.8	1.1	319.0	60.0	35.0	22.5	16.1	3.3	7.3
		135.9	35.9	1.1	27.0	60.0	125.0	25.4	16.1	3.3	
		136.1	36.2	1.1	344.0	60.0	40.0	22.5	16.1	3.3	
	F53	135.9	35.4	1.0	291.0	90.0	35.0	17.2	14.0	2.9	7.2
		135.8	35.5	1.0	310.0	90.0	35.0	11.4	14.0	2.9	
		135.7	35.6	1.0	319.0	90.0	35.0	31.3	14.0	2.9	
	F54	135.1	35.6	1.1	332.0	90.0	35.0	57.6	13.9	2.8	7.2
Virtual Tsunami (MLIT)	F55	134.4	35.8	1.1	261.0	60.0	215.0	69.0	16.0	4.0	7.5
		133.7	35.7	1.1	249.0	60.0	215.0	25.8	16.0	4.0	
	F56	133.0	35.6	1.1	217.0	60.0	143.0	7.1	16.0	2.8	7.2
		132.9	35.6	1.1	268.0	60.0	215.0	42.4	16.0	2.8	
	F57	132.4	35.5	1.2	271.0	60.0	215.0	72.4	16.0	4.2	7.5
		131.6	35.5	1.2	235.0	60.0	145.0	30.1	16.0	4.2	
	F58	131.5	34.7	1.1	329.0	90.0	325.0	50.1	13.9	2.6	7.1
	F59	131.1	34.1	1.1	310.0	90.0	325.0	87.9	13.9	3.5	7.4
	F60	130.9	33.4	1.0	321.0	90.0	325.0	136.9	14.0	4.6	7.6

References

1. Davis, I.; Izadkhah, Y.O. Tsunami early warning system (EWS) and its integration within the chain of seismic safety. *Disaster Prev. Manag. Int. J.* **2008**, *17*, 281–291. [CrossRef]
2. Wächter, J.; Babeyko, A.; Fleischer, J.; Häner, R.; Hammitzsch, M.; Kloth, A.; Lendholt, M. Development of tsunami early warning systems and future challenges. *Nat. Hazards Earth Syst. Sci.* **2012**, *12*, 1923–1935. [CrossRef]
3. Schlurmann, T.; Kongko, W.; Goseberg, N.; Natawidjaja, D.H.; Sieh, K. Near-field tsunami hazard map Padang, West Sumatra: Utilizing high resolution geospatial data and reasonable source scenarios. In Proceedings of the Coastal Engineering Conference, Shanghai, China, 30 June–5 July 2010; American Society of Civil Engineers: Reston, VA, USA, 2010.

4.   Kurowski, M.J.; Hedley, N.; Clague, J.J. An assessment of educational tsunami evacuation map designs in Washington and Oregon. *Nat. Hazards* **2011**, *59*, 1205–1223. [CrossRef]

5.   Fukutani, Y.; Suppasri, A.; Immamura, F. Stochastic analysis and uncertainty assessment of tsunami wave height using a random source parameter model that targets a Tohoku-type earthquake fault. *Stoch. Environ. Res. Risk Assess.* **2015**, *29*, 1763–1779. [CrossRef]

6.   Park, H.; Cox, D.T.; Barbosa, A.R. Probabilistic Tsunami Hazard Assessment (PTHA) for Resilience Assessment of a Coastal Community. *Nat. Hazards* **2018**, *94*, 1117–1139. [CrossRef]

7.   Satake, K. Effects of bathymetry of tsunami propagation: Application of ray tracing to tsunamis. *Pure Appl. Geophys.* **1988**, *126*, 27–36. [CrossRef]

8.   Sandanbata, O.; Watada, S.; Satake, K.; Fukao, Y.; Sugioka, H.; Ito, A.; Shiobara, H. Ray tracing for dispersive tsunamis and source amplitude estimation based on Green's law: Application to the 2015 volcanic tsunami earthquake near Torishima, south of Japan. *Pure Appl. Geophys.* **2018**, *175*, 1371–1385. [CrossRef]

9.   Woods, M.T.; Okal, E.A. Effect of variable bathymetry on the amplitude of teleseismic tsunamis: A ray-tracing experiment. *Geophys. Res. Lett.* **1987**, *14*, 765–768. [CrossRef]

10.   Goto, K.; Chagué-Goff, C.; Goff, J.; Jaffe, B. The future of tsunami research following the 2011 Tohoku-oki event. *Sediment. Geol.* **2012**, *282*, 1–13. [CrossRef]

11.   Mas, E.; Koshimura, S.; Suppasri, A.; Matsuoka, M.; Matsuyama, M.; Yoshii, T.; Jimenez, C.; Yamazaki, F.; Imamura, F. Developing Tsunami fragility curves using remote sensing and survey data of the 2010 Chilean Tsunami in Dichato. *Nat. Hazards Earth Syst. Sci.* **2012**, *12*, 2689–2697. [CrossRef]

12.   Cho, Y.S.; Jin, S.B.; Lee, H.J. Safety analysis of Ulchin nuclear power plant against Nihonkai-Chubu earthquake tsunami. *Nucl. Eng. Des.* **2004**, *228*, 393–400. [CrossRef]

13.   Manshinha, L.; Smylie, D.E. The displacement fields of inclined faults. *Bull. Seismol. Soc. Am.* **1971**, *61*, 1433–1440. [CrossRef]

14.   Ministry of Land, Infrastructure, Transport and Tourism. *Report of the Study Group on Investigation and Assessment of Large-Scale Earthquake in the Sea of Japan*; Ministry of Land, Infrastructure, Transport and Tourism: Tokyo, Japan, 2014. (In Japanese)

15.   Korean Peninsula Energy Development Organization. *Estimation of Tsunami Height for KEDO LWR Project*; Korea Power Engineering Company, Inc.: Inchon, Korea, 1999.

16.   Power, W.; Downes, G.; Stirling, M. Estimation of tsunami hazard in New Zealand due to south American earthquakes. *Pure Appl. Geophys.* **2007**, *164*, 547–564. [CrossRef]

17.   Park, H.; Cox, D.T. Probabilistic assessment of near-field tsunami hazards: Inundation depth, velocity, momentum flux, arrival time, and duration applied to Seaside, Oregon. *Coast. Eng.* **2016**, *117*, 79–96. [CrossRef]

18.   Geist, E.L.; Parsons, T. Probabilistic analysis of tsunami hazards. *Nat. Hazards* **2006**, *37*, 277–314. [CrossRef]

19.   Japan Society of Civil Engineers. *Tsunami Assessment Technique for Nuclear Power Plant 2016*; Japan Society of Civil Engineers: Tokyo, Japan, 2016. (In Japanese)

20.   Wang, X. *User manual for COMCOT version 1.7 (first draft)*; Cornel University: Ithaca, NY, USA, 2009; Volume 65, p. 480.

21.   Sohn, D.-H.; Ha, T.; Cho, Y.-S. Distant tsunami simulation with corrected dispersion effects. *Coast. Eng. J.* **2009**, *51*, 123–131. [CrossRef]

22.   Liu, P.L.F.; Cho, Y.-S.; Yoon, S.B.; Seo, S.N. Numerical simulations of the 1960 Chilean tsunami propagation and inundation at Hilo, Hawaii. In *Tsunami: Progress in Prediction, Disaster Prevention and Warning*; Tsuchiya, Y., Shuto, N., Eds.; Springer: Dordrecht, The Netherlands, 1994; Volume 4, pp. 99–115.

23.   Gusman, A.R.; Satake, K.; Shinohara, M.; Sakai, S.I.; Tanioka, Y. Fault slip distribution of the 2016 Fukushima earth-quake estimated from tsunami waveforms. *Pure Appl. Geophys.* **2017**, *174*, 247–257. [CrossRef]

24.   Cho, Y.S.; Hwang, H.S.; Kim, J.Y.; Kwon, H.H. Development of Hazard Map with probable maximum tsunamis. *J. Coast. Res.* **2016**, *75*, 1057–1061. [CrossRef]

25.   Kim, K.H.; Cho, Y.S.; Kwon, H.H. An integrated Bayesian approach to the probabilistic tsunami risk model for the location and magnitude of earthquakes: Application to the eastern coast of the Korean Peninsula. *Stoch. Environ. Res. Risk Assess.* **2018**, *32*, 1243–1257. [CrossRef]

26.   Yoon, S.B.; Kim, S.C.; Baek, U.; Bae, J.S. Effects of bathymetry on the propagation of tsunamis towards the east coast of Korea. *J. Coast. Res.* **2014**, *70*, 332–337. [CrossRef]

27.   European Commission. New Approach to Reactor Safety Improvements (NARSIS) Project (WP1). 2020. Available online: https://ec.europa.eu/research/participants/documents/downloadPublic?documentIds=080166e5d311ea9a&appId=PPGMS (accessed on 16 October 2022).